I002

# Effects of Permeability Barriers and Pore Fluids on S-wave Attenuation

B. Quintal* (ETH Zurich), M. Frehner (ETH Zurich), S.M. Schmalholz (University of Lausanne), H. Steeb (Ruhr University Bochum) & E.H. Saenger (ETH Zurich)

## SUMMARY

We numerically perform stress relaxation experiments using Biot's equations for consolidation of poroelastic media to study seismic attenuation of S-waves caused by wave-induced fluid flow. Our model consists of periodically distributed mesoscopic-scale circular heterogeneities with lower porosity and permeability than the background, which contains 80% of the total pore space of the medium. This model represents a hydrocarbon reservoir, where the background is fully saturated with oil or gas (or water, for comparison), and the low porosity heterogeneities are always saturated with water. Varying the dry bulk and shear moduli in the medium, a tendency is observed in the relative behavior of the S-wave attenuation among the different saturation scenarios. First, in the gas-saturated media the S-wave attenuation is very low and much lower than in the oil-saturated or in the fully water-saturated media. Second, at low frequencies the S-wave attenuation is significantly higher in the oil-saturated media than in the fully water-saturated media. Additionally, we observed that impermeable barriers in the background can cause a significant increase in S-wave attenuation. Based on the theory of wave-induced fluid flow, our results suggest that S-wave attenuation could be used as an indicator of fluid content and permeability changes in a reservoir.

## Introduction

We present a numerical study of S-wave attenuation caused by wave-induced fluid flow. At low seismic frequencies (1-100 Hz), wave-induced fluid flow caused by fluid pressure differences between mesoscopic-scale heterogeneities is a major cause of attenuation in a porous rock (Pride et al., 2004). The mesoscopic scale is the scale much larger than the pore size but much smaller than the wavelength. These heterogeneities can occur in fluid and/or solid frame properties. Pore fluid effects have been studied for P-wave attenuation in patchy saturated models, for which the rock frame is homogeneous and heterogeneities occur in fluid saturation (e.g., Quintal et al., 2009). In such patchy saturated models with homogeneous rock frame, S-waves are not attenuated. Attenuation of S-waves occurs as a consequence of heterogeneities in the solid frame, but is also function of fluid properties (Berryman and Wang, 2001). Here we investigate the effects of the pore fluid on S-wave attenuation.

## Material and methods

We numerically simulate stress relaxation experiments by solving Biot's equations for consolidation of poroelastic media (Biot, 1941). Because no inertia terms appear in these equations, the computed attenuation is solely due to flow of the viscous fluid, which is controlled by the gradient of the pore fluid pressure. We use the equations for consolidation in the u-p formulation, which allows us to implement the boundary conditions for zero fluid flow (undrained test) in the weak formulation. Therefore, all our simulations are performed using a numerical model with undrained boundaries. The algorithm employs the finite-element method and an unstructured mesh with triangular elements consisting of seven nodal points. A detailed description is given by Quintal et al. (2011). Benchmark tests show that it is suited to accurately determine the complex moduli over a broad frequency range.

We perform relaxation tests on 2D poroelastic samples with periodically distributed mesoscopic-scale heterogeneities. The heterogeneities have low permeability and low porosity and are embedded in a continuous background medium of high permeability and high porosity. The heterogeneities are always fully saturated with water and the background is saturated with oil, gas, or water. This model can represent a hydrocarbon reservoir, where water (wetting fluid) is not displaced from regions of small pores due to capillary effects. The unit cell of this model is a 40-cm side square with the heterogeneity located in the center. The radius of the circular heterogeneity is 16 cm. The circle occupies 50% of the unit cell. Because of the different porosities in the heterogeneity and in the background, the pore space in the background corresponds to 80% of the total pore space in the medium. We then perform simulations considering the three saturation scenarios: oil-saturated medium (80% oil, 20% water); gas-saturated medium (80% gas, 20% water); and fully water-saturated medium. Four sets of parameters are considered for the solid frame, differing only in the bulk and the shear moduli of the dry frame. Fluid and solid parameters are given in Tables 2 and 3, with symbols defined in Table 1. The parameters for the solid frame were arbitrarily combined to represent strong variations in the rock that could be related, for example, to the degree of cementation or mineralogical composition. We perform two sets of relaxation experiments using two numerical models consist of (1) 25 unit cells spatially arranged in a 5×5 array and (2) a single unit cell.

Each relaxation experiment consists of a simple-shear test, illustrated in Figure 1. A time-dependent smoothed-step function (e.g., Masson and Pride, 2007) is attributed at the boundaries of the model to the displacement, as indicated in Figure 1. Time-dependent shear strain and stress in the x-z-directions are obtained from this experiment. A partial time derivative is applied to these results and the time-dependent shear strain and stress rates in the x-z-direction are converted into the frequency domain yielding, $\hat{\varepsilon}_{xz}$ and $\hat{\sigma}_{xz}$, respectively. The shear modulus, $\mu$, is then calculated with

$$\mu = \hat{\sigma}_{xz}/2\hat{\varepsilon}_{xz}. \qquad (1)$$

The complex and frequency-dependent modulus $\mu$ is used to calculate the S-wave quality factor with

$$Q_S = \mathrm{Re}(\mu)/\mathrm{Im}(\mu). \qquad (2)$$

The inverse of $Q$ is a measure of attenuation. S-wave attenuation in our experiments is caused by fluid flow induced by pressure differences between regions of different compliances.
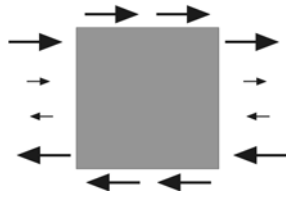
**Figure 1.** *Sketch of the simple-shear experiment. The arrows indicate direction and magnitude of the displacements applied in x-direction at the boundaries of the model. At the left and right boundaries, the magnitude has a linear dependence on the z-direction. The displacement in the z-direction is fixed to zero at all the four boundaries.*

## Simulations and results

Figure 4 shows snapshots of the two simple-shear experiments for the oil-saturated medium and Case A. The snapshots in Figure 2a correspond to the simple-shear test with a numerical model composed of a 5×5 array of unit cells. The shear strain and stress calculated from this experiment are averaged over the area of a single cell located at the center of the array. This is done to avoid the effect of the undrained boundaries and to simulate a medium with periodically distributed circular heterogeneities embedded in a homogeneous background. The snapshots in Figure 2b correspond to the simple-shear test with a numerical model consisting of only one cell. The shear strain and stress are averaged over the area of the unit cell. The results from the simulations illustrated in Figures 2a and 2b are, respectively, shown in Figures 3a and 3b (only the curves for Case A and oil saturation).
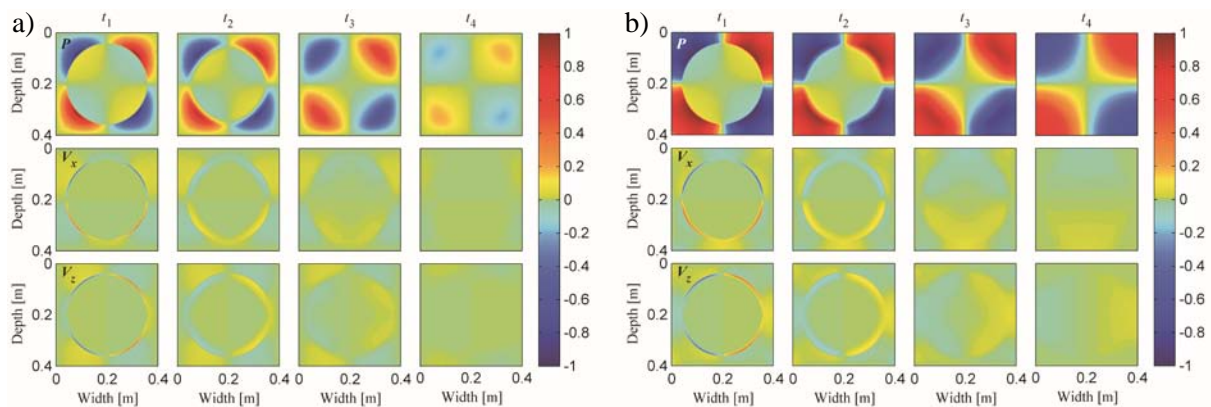


**Figure 2.** *Snapshots at times $t_1$, $t_2$, $t_3$, and $t_4$ of the pore fluid pressure field (P), and the fluid velocities in the x- and z-direction ($V_x$ and $V_z$), normalized by their maximum values, for the simple-shear experiments with the numerical model consisting of (a) 25 unit cells spatially arranged in a 5×5 array, and (b) a single unit cell. The fluid and solid frame properties correspond to oil saturation in the background and Case A (Tables 2 and 3).*

The results from the simple-shear tests, for Cases A-D and the three saturation scenarios, with a numerical model consisting of a 5×5 array of unit cells and for a single unit cell, are shown in Figures 3a and 3b, respectively. During the simple-shear experiments, there is a significant pressure gradient across the boundaries between unit cells in a periodic medium (e.g., Figures 2a and 2b) and, therefore, the fluid flow across the boundaries is significant. This causes the results of the simple-shear test using a periodic model (5×5 array of unit cells, Figure 3a) to be considerably different than the results of such a test using a single unit cell (Figure 3b). The S-wave attenuation is significantly higher when the numerical model consists of a single unit cell. The difference between the two models causing such an increase in S-wave attenuation is the undrained boundary condition. The numerical model consisting of a single unit cell can represent a medium with periodically distributed circular heterogeneities having impermeable barriers between the unit cells. The numerical model consisting of a 5x5 array of unit cells represents a periodic medium having no such barriers in the background. The impermeable barriers cause an increase of about one order of magnitude in the S-wave attenuation, and also a shift of about one order of magnitude of the $Q_S$ curves to lower frequencies.

We also observe in Figure 3 that the value of Re($\mu$) at the low-frequency (quasi-static) limit is independent on the properties of the saturating fluid. However, for higher frequencies, it changes with changing fluid saturation. This difference (dispersion) is a consequence of S-wave attenuation,

according to the Kramers-Kronig relations. Moreover, despite the differences in the rock frame properties in Cases A-D or the presence of impermeable barriers, we observe approximately the same relative behavior of the S-wave attenuation among the three different saturation scenarios in Figure 3. In other words, all eight plots for $Q_S$ exhibit a similar relative position of the three curves. One feature of this relative behavior is that the S-wave attenuation in the gas-saturated media is very low and much lower than in the oil-saturated or in the fully water-saturated media. Second, at low frequencies, the S-wave attenuation is significantly higher in the oil-saturated media than in the fully water-saturated media, although its maximum value is higher in the fully water-saturated media.
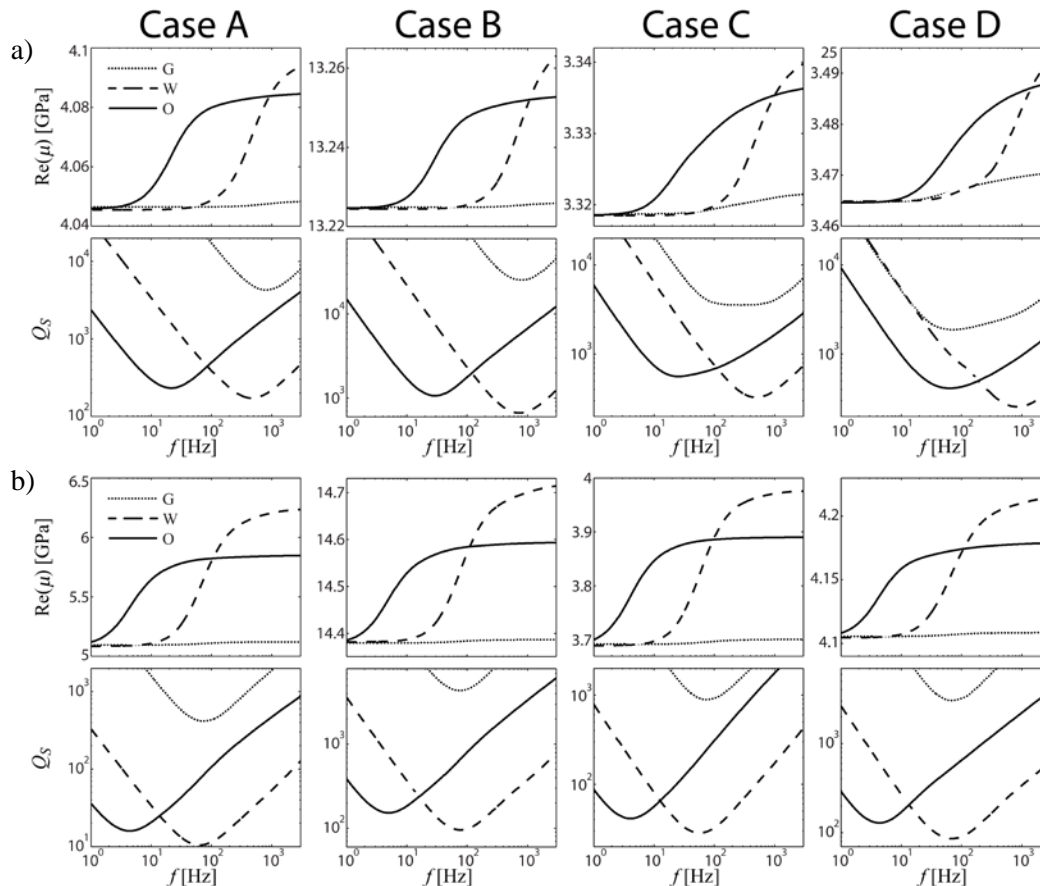


**Figure 3.** *Numerical results for the real part of the shear modulus, μ, and the S-wave quality factor, $Q_S$, obtained from simple-shear tests using (a) a numerical model consisting of a 5×5 array of unit cells and (b) a numerical model consisting of a single unit cell. The properties of the fluids and solid frame are given in Tables 2 and 3. The legend terms refer to the three saturation scenarios: 80% gas, 20% water (G); 100% water (W); and 80% oil, 20% water (O).*

**Conclusions**

Relaxation experiments were numerically performed to calculate S-wave attenuation due to wave-induced fluid flow in poroelastic media containing periodically distributed heterogeneities embedded in a permeable homogeneous background. We studied the influence of undrained boundary conditions for numerical models consisting of either a single unit cell or an array of unit cells of such a periodic medium. We observed that the undrained boundary condition causes a significant increase in S-wave attenuation when the numerical model consists of only a single unit cell. Shear relaxation experiments simulated to calculate S-wave attenuation in a periodic medium with permeable homogeneous background require numerical models composed of several unit cells or another type of boundary condition. This also shows that a fluid-saturated medium will have significantly increased S-wave attenuation in regions surrounded by impermeable barriers. This suggests that S-wave attenuation could be an indicator of permeability changes in, for example, fracturing operations.

We explained the dependence of the shear modulus on the fluid saturation at frequencies higher than the quasi-static limit by S-wave attenuation due to wave-induced fluid flow at the mesoscopic scale. The S-wave attenuation due to this mechanism in a medium with heterogeneous solid frame exhibits a consistent tendency in its relative behavior among different saturation scenarios (80% oil, 20% water; 80% gas, 20% water; and 100% water). First, the S-wave attenuation in the gas-saturated media is very low and much lower than in the oil-saturated or in the fully water-saturated media. Second, at low frequencies, the S-wave attenuation is significantly higher in the oil-saturated media than in the fully water-saturated media. This tendency is observed for media containing periodically distributed heterogeneities, considering four sets of rock frame parameters. Based on these relative behaviors, we suggest that S-wave attenuation could be used as an indicator of fluid content in a reservoir. For example, spectral decomposition could be applied to seismic S-wave data to help distinguish between oil and water content, because at low frequencies attenuation of S-waves tends to be higher in oil-saturated (80% oil, 20% water) media than in media fully saturated with water, according to the physical mechanism of wave-induced fluid flow.

## Acknowledgements

## References

Berryman, J. G., and H. F. Wang, 2001, Dispersion in poroelastic systems: Phys. Rev. E, 64, 011303.

Biot, M. A., 1941, General theory of three-dimensional consolidation: J. Appl. Phys., 12, 155-164.

Masson, Y. J., and S. R. Pride, 2007, Poroelastic finite-difference modeling of seismic attenuation and dispersion due to mesoscopic-scale heterogeneity: J. Geophys. Res., 112, B03204.

Pride, S. R., J. G. Berryman, and J. M. Harris, 2004, Seismic attenuation due to wave-induced flow: J. Geophys. Res., 109, B01201.

Quintal, B., S. M. Schmalholz, and Y. Y. Podladchikov, 2009, Low-frequency reflections from a thin layer with high attenuation caused by interlayer flow: Geophysics, 74, N15-N23.

Quintal, B., H. Steeb, M. Frehner, and S. M. Schmalholz, 2011, Quasi-static finite-element modeling of seismic attenuation and dispersion due to wave-induced fluid flow in poroelastic media: J. Geophys. Res., 116, B01201.

Table 1. Symbols for the petrophysical parameters given in Tables 2 and 3.

| Symbol | Definition |
|--------|------------|
| $\rho_s$ | Density of the grains |
| $K_s$ | Bulk modulus of the grains |
| $\phi$ | Porosity |
| $k$ | Permeability |
| $K_d$ | Bulk modulus of the dry frame |
| $\mu_d$ | Shear modulus of the dry frame |
| $\rho_f$ | Density of the fluid |
| $\eta$ | Viscosity of the fluid |
| $K_f$ | Bulk modulus of the fluid |

Table 2. Physical properties of the fluids.

| Fluid | Water | Oil | Gas |
|-------|-------|-----|-----|
| $\rho_f$ (kg/m$^3$) | 1010 | 880 | 160 |
| $\eta$ (Pa·s) | 0.001 | 0.02 | $2\times10^{-5}$ |
| $K_f$ (GPa) | 2.4 | 1.4 | 0.04 |

Table 3. Physical properties of the solid frame.

| Region | Heterogeneity | Background |
|--------|---------------|------------|
| $\rho_s$ (kg/m$^3$) | 2700 | 2700 |
| $K_s$ (GPa) | 40 | 48 |
| $\phi$ (%) | 6 | 26 |
| $k$ (mD) | 40 | 1000 |
| Case A | | |
| $K_d$ (GPa) | 36 | 4 |
| $\mu_d$ (GPa) | 32 | 2 |
| Case B | | |
| $K_d$ (GPa) | 36 | 10 |
| $\mu_d$ (GPa) | 32 | 8 |
| Case C | | |
| $K_d$ (GPa) | 10 | 4 |
| $\mu_d$ (GPa) | 8 | 2 |
| Case D | | |
| $K_d$ (GPa) | 4 | 10 |
| $\mu_d$ (GPa) | 2 | 8 |